

# Contributions of Atmosphere–Ocean Interaction and Low-Frequency Variation to Intensity of Strong El Niño Events since 1979

XIAOFAN LI

*School of Earth Sciences, Zhejiang University, Hangzhou, Zhejiang, China*

ZENG-ZHEN HU

*NOAA/NCEP/NWS/Climate Prediction Center, College Park, Maryland*

BOHUA HUANG

*Center for Ocean–Land–Atmosphere Studies, and Department of Atmospheric, Oceanic, and Earth Sciences, College of Science, George Mason University, Fairfax, Virginia*

(Manuscript received 6 April 2018, in final form 6 December 2018)


## ABSTRACT

Evolutions of oceanic and atmospheric anomalies in the equatorial Pacific during four strong El Niños (1982/83, 1991/92, 1997/98, and 2015/16) since 1979 are compared. The contributions of the atmosphere–ocean coupling to El Niño–associated sea surface temperature anomalies (SSTA) are identified and their association with low-level winds as well as different time-scale variations is examined. Although overall SSTA in the central and eastern equatorial Pacific is strongest and comparable in the 1997/98 and 2015/16 El Niños, the associated subsurface ocean temperature as well as deep convection and surface wind stress anomalies in the central and eastern equatorial Pacific are weaker during 2015/16 than that during 1997/98. That may be associated with a variation of the wind–SST and wind–thermocline interactions. Both the wind–SST and wind–thermocline interactions play a less important role during 2015/16 than during 1997/98. Such differences are associated with the differences of the low-level westerly wind as well as the contribution of different time-scale variations in different events. Similar to the interannual time-scale variation, the intraseasonal–interseasonal time-scale component always has positive contributions to the intensity of all four strong El Niños. Interestingly, the role of the interdecadal-trend time-scale component varies with event. The contribution is negligible during the 1982/83 El Niño, negative during the 1997/98 El Niño, and positive during the 1991/92 and 2015/16 El Niños. Thus, in addition to the atmosphere–ocean coupling at intraseasonal to interannual time scales, interdecadal and longer time-scale variations may play an important and sometimes crucial role in determining the intensity of El Niño.

## 1. Introduction

Although various theories about El Niño–Southern Oscillation (ENSO) have been proposed and significant progress has been made in understanding the phenomena in recent decades (Philander 1990; Jin 1997a,b; Wang 2001; Sarachik and Cane 2010; National Research Council 2010; An and Kim 2017; Santoso et al. 2017), unsuccessful predictions of the ENSO cycle during

2010–14 and 2017/18 are good examples to demonstrate the challenges of operational ENSO forecast (<https://iri.columbia.edu/our-expertise/climate/ens0>; Zhang et al. 2013; Zhu et al. 2016; Huang et al. 2017). Moreover, our capability in predicting ENSO (or the ENSO-prediction skill) did not show a steady increase with time progress, instead showing a decrease after 1999/2000 (Wang et al. 2010; Barnston et al. 2012), although the oceanic observations increased substantially in the last period (Kumar et al. 2015). Also, our state-of-the-art operational climate forecast systems have little skill in predicting ENSO evolution during its development phase, and most of the skill actually comes from predicting evolution at its decay phase (Zheng et al. 2016),

 Denotes content that is immediately available upon publication as open access.

Corresponding author: X. Li, xiaofanli@zju.edu

DOI: 10.1175/JCLI-D-18-0209.1

© 2019 American Meteorological Society. For information regarding reuse of this content and general copyright information, consult the [AMS Copyright Policy](https://www.ametsoc.org/PUBSReuseLicenses) ([www.ametsoc.org/PUBSReuseLicenses](https://www.ametsoc.org/PUBSReuseLicenses)).

implying an extreme and inherent challenge to predicting the initiation of an event (Hu et al. 2019).

Because ENSO plays a dominant role in the tropical Pacific climate variability at seasonal–interannual time scales, and is also the largest source of predictability of global climate variability (National Research Council 2010; Wang et al. 2010, 2013), further attempts to understand ENSO and improve its prediction is necessary. Moreover, correctly forecasting ENSO evolution is the underpinning for skillful seasonal climate forecasts over some land regions [such as North America (Ropelewski and Halpert 1987) and East Asia (Wu et al. 2003; Liang et al. 2019; National Research Council 2010)] that directly affect people's life and property as well as social development.

Occurrence of the extremely strong El Niño in 2015/16 and its unusual impact on some regional climates (e.g., it did not relieve the California drought as widely expected from historical event statistics; Kumar and Chen 2017) have triggered analyses to compare the similarities and differences among strong El Niños in history (Santoso et al. 2017). For example, Paek et al. (2017), Ren et al. (2017), and Lim et al. (2017) compared various aspects of the evolution of atmospheric and oceanic anomalies during the 1997/98 and 2015/16 El Niño (and 1982/83) events. Santoso et al. (2017) indicated the spatial pattern difference for both sea surface temperature anomalies (SSTAs) and rainfall anomalies associated with the 1982/83, 1997/98, and 2015/16 El Niños. Compared with the 2015/16 El Niño, both SSTAs and rainfall anomalies in the mature phase of the 1982/83 and 1997/98 events were present more eastward. Paek et al. (2017) argued that the 1997/98 and 2015/16 events involved different physical processes: The former was driven by basin-wide thermocline variations, whereas the latter was largely affected by subtropical forcing. Tseng et al. (2017) emphasized the connection between extratropical anomalies (such as the warm blob in the northeastern Pacific) and the occurrence of the 2015/16 El Niño.

These previous works have clearly demonstrated the similarities and differences of atmosphere and oceanic variability and underlying dynamics among these strong El Niño events. In this work, in addition to showing the evolution of oceanic and atmospheric anomalies in the equatorial Pacific during four strong El Niños (1982/83, 1991/92, 1997/98, and 2015/16) since 1979, we identify contributions of the atmosphere–ocean coupling to El Niño–associated SSTAs during these strong El Niños. Furthermore, low-level winds, as well as time-scale decompositions of Niño-3.4 SSTAs are analyzed to understand the differences of the atmosphere–ocean coupling and relative importance of different time-scale

components during these events. The rest of the paper is organized as follows. The data used in this work are introduced in section 2. Section 3 shows the results, including the evolution of oceanic and atmospheric anomalies in the equatorial Pacific during the four strong El Niños, contributions of the atmosphere–ocean interactions to El Niño–associated SSTA, and the relative importance of different time-scale components to the four strong El Niños. A summary and discussion are given in section 4.

## 2. Data

Monthly mean of SST is from Optimum Interpolation SST, version 2 (OISSTv2, hereafter OIv2), on a  $1^\circ \times 1^\circ$  resolution (Reynolds et al. 2002). The Niño-3 and Niño-3.4 indices are defined as the averaged SSTA in the regions of ( $5^\circ\text{S}$ – $5^\circ\text{N}$ ,  $150^\circ$ – $90^\circ\text{W}$ ) and ( $5^\circ\text{S}$ – $5^\circ\text{N}$ ,  $170^\circ$ – $120^\circ\text{W}$ ), respectively. The Niño-3.4 index is used to measure the evolution and intensity of ENSO. The ENSO year definition follows that of the Climate Prediction Center (CPC) of NOAA based on a 3-month running mean Niño-3.4 index ([http://www.cpc.ncep.noaa.gov/products/analysis\\_monitoring/ensostuff/ensoyears.shtml](http://www.cpc.ncep.noaa.gov/products/analysis_monitoring/ensostuff/ensoyears.shtml)). There are in total 11 El Niño events during 1979–2017: 1979/80, 1982/83, 1986–88, 1991/92, 1994/95, 1997/98, 2002/03, 2004/05, 2006/07, 2009/10, and 2015/16. Here, we focus on strong El Niño events during 1979–2017. Based on the intensity classification of NOAA CPC, strong El Niño events are referred to as amplitudes of 3-month mean Niño-3.4 SSTAs larger than  $1.5^\circ\text{C}$  in December–February (DJF). According to this criteria, there were four strong El Niño events (1982/83, 1991/92, 1997/98, and 2015/16; Fig. 1). The 1986–88 El Niño is not classified as strong event since the amplitude of Niño-3.4 SSTAs in DJF is smaller than  $1.5^\circ\text{C}$ , and the maximum 3-monthly mean Niño-3.4 SSTA occurred in late summer and early autumn with an amplitude of  $1.6^\circ\text{C}$ . In addition, Huang et al. (2013, 2016) noted that there are substantial differences (biases) among various analyzed SST datasets, which sometimes can be even larger than  $0.5^\circ\text{C}$  in the Niño-3.4 region. Such differences or biases in SST data can affect the estimate of El Niño amplitude to some extent (Santoso et al. 2017). The different spatial distribution patterns of SSTAs in the tropical Pacific in various El Niño years is another factor affecting the magnitude estimation based on a given index (e.g., Niño-3.4).

Monthly mean surface wind stress and the  $20^\circ\text{C}$  isotherm (D20) analyzed in this work are from the Global Ocean Data Assimilation System (GODAS) on a  $1^\circ \times 1^\circ$  grid (Behringer 2007). Monthly mean surface heat flux and 6-hourly winds at 1000 hPa are from NCEP–DOE

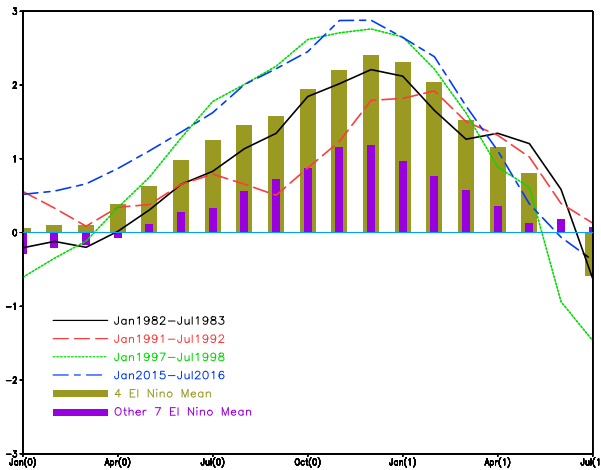


FIG. 1. Time evolution of monthly mean Niño-3.4 SSTAs during January 1982–July 1983 (dark solid line), January 1991–July 1992 (red dashed line), January 1997–July 1998 (green solid line), January 2015–July 2016 (blue dashed line), and their average (thick bars). The thin bars represent the average for seven weak-to-moderate El Niños. The unit is  $^{\circ}\text{C}$ .

reanalysis, also on a  $1^{\circ} \times 1^{\circ}$  grid (Kanamitsu et al. 2002). Outgoing longwave radiation (OLR) data on a  $2.5^{\circ} \times 2.5^{\circ}$  grid are from Liebmann and Smith (1996). Except for November 1981–June 2018 for OIv2, all the other data are for January 1979–June 2018. To make up the unavailability of the OIv2 data in January 1979–October 1981, ocean temperature at the top layer of GODAS is used as an alternative. The anomalies are referred to as the departures from monthly climatologies during January 1981–December 2010.

The heat budget in the ocean mixed layer (OML) is also diagnosed using data from GODAS (Huang et al. 2010; Hu et al. 2016). Following Huang et al. (2010), the tendency of ocean temperature of OML is defined as

$$\frac{\partial T}{\partial t} = Q_u + Q_v + Q_w + Q_{zz} + Q_q + R,$$

where  $\partial T/\partial t$  is the temperature tendency of OML;  $Q_u$  and  $Q_v$  are zonal and meridional advection, respectively;  $Q_w$  ( $Q_{zz}$ ) is vertical entrainment (diffusion);  $Q_q$  is adjusted surface heat flux, which is the net surface heat flux plus heat flux correction minus the penetrative shortwave radiation (Huang et al. 2010); and  $R$  is the residual term and contains the effect of horizontal heat diffusion and the contributions of the submonthly processes.

To display the time-scale-dependent variability of the Niño-3.4 index, ensemble empirical mode decomposition (EEMD) is applied (Wu and Huang 2009). Different from the Fourier-transform-based time-series analysis that uses a priori “global” basis functions of rigid periods, EEMD is adaptive and derives optimal

frequencies for decomposing data from the data itself, which provides a natural filter to separate components of different time scales (Huang et al. 1998; Huang and Wu 2008). To measure the atmosphere–ocean coupling strength, we compute the wind–SST and wind–thermocline interactions, key processes for ENSO growth and decay, which is defined as the regressions of zonal wind stress anomalies onto the Niño-3 SST and zonal gradient of D20 anomalies, respectively (Lloyd et al. 2009).

### 3. Results

#### a. Evolution of strong El Niños

From Fig. 1, we note that the evolution pattern and peak time are similar for the means of the four strong El Niños (thick bar) and of the seven weak-to-moderate El Niños (thin bar). For the four strong El Niños, the monthly peak value of Niño-3.4 SSTA is slightly larger in the 2015/16 El Niño than in the 1997/98 El Niño. For the 1982/83 and 1991/92 El Niños, the monthly peak values of Niño-3.4 SSTAs are smaller than those in 1997/98 and 2015/16. However, the results could change if a different index is used to make the comparison because of the spatial distribution difference of SSTAs in different events. For example, if the Niño-3 index is used for comparison, the 1982/83 El Niño is more similar to 1997/98 than to 1991/92 events in amplitude. Paek et al. (2017) indicated that the 1997/98 event is the strongest eastern Pacific (EP) El Niño, while the 2015/16 event is the strongest mixed EP and central Pacific (CP) El Niño ever recorded. However, Huang et al. (2016) argued that there are large uncertainties and biases in observed/analyzed SST datasets, which affect both the ranking and definition of El Niño events.

In fact, beyond the similarity of the composites of the four strong El Niños (Fig. 2e) and of the seven weak-to-moderate El Niños (Fig. 2f) to the composites of Rasmusson and Carpenter (1982), there are some obvious differences for atmosphere and ocean anomalies associated with the four strong El Niño events (Figs. 2a–d). For instance, overall positive SSTA in the central and eastern equatorial Pacific is the largest in 1997/98 and smallest in 1991/92. Also, in contrast to almost stationary variation during 1982/83 and 1991/92, SSTAs in the central and eastern equatorial Pacific during 1997/98 and 2015/16 show pronounced westward propagation. For the spatial pattern of positive SSTAs along the equator, the maximum SSTA is located farther westward during 1991/92 and 2015/16 compared with 1982/83 and 1997/98. The former are more analogous to the so-called CP (or warm pool, Modoki) El Niño event, while the latter

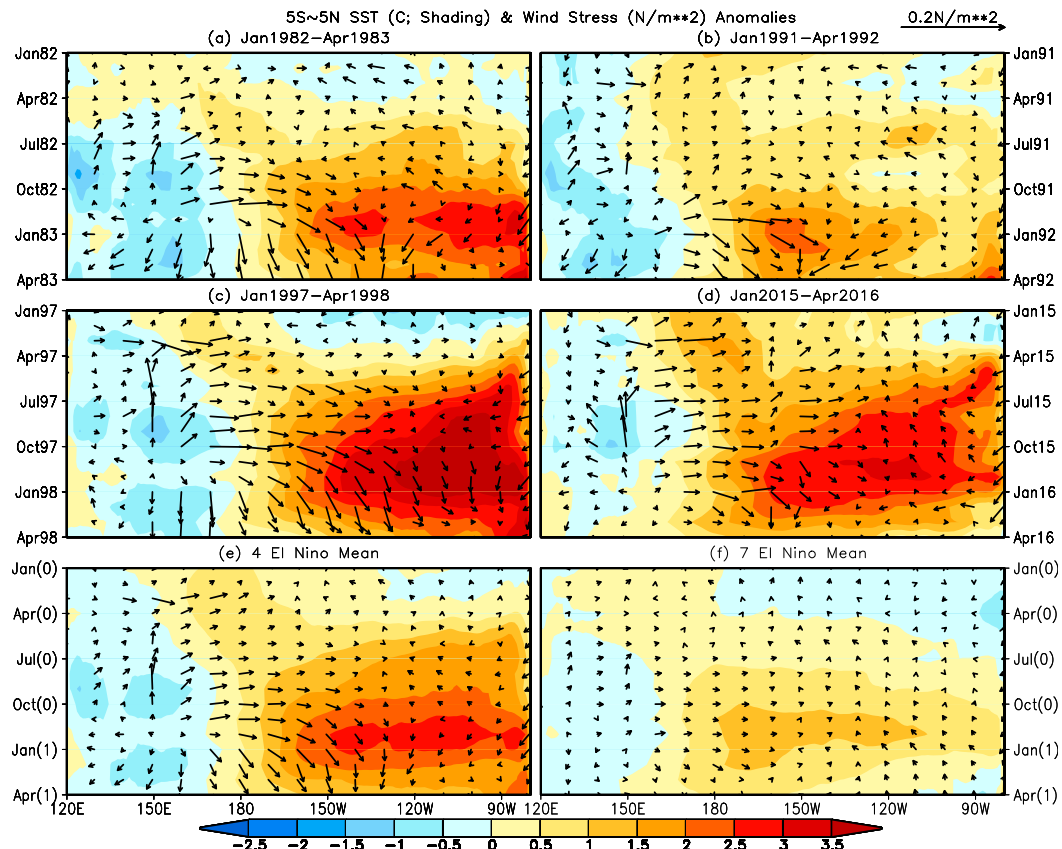


FIG. 2. Time evolution of monthly mean SST (shading) and wind stress (vector) anomalies averaged in  $5^{\circ}\text{S}$ – $5^{\circ}\text{N}$  during (a) January 1982–April 1983, (b) January 1991–April 1992, (c) January 1997–April 1998, and (d) January 2015–April 2016 as well as the average for (e) the four strong El Niños and (f) seven weak–moderate El Niños. The unit is  $^{\circ}\text{C}$  for SST and  $\text{N m}^{-2}$  for wind stress.

ones are EP (or cold tongue, convention) events (Ashok et al. 2007; Kao and Yu 2009; Kug et al. 2010; Hu et al. 2012; Paek et al. 2017). Among the four events, the surface wind stress anomalies are the strongest during 1997/98 and the weakest during 1991/92. The wind stress anomalies also have longer persistence during 1997/98 than 1991/92.

From the composite of the four strong El Niños (Figs. 2e, 3e) and of the seven weak–moderate El Niños (Figs. 2f, 3f), we see coupling features among surface zonal wind, OLR, and thermocline depth (D20) along the equatorial Pacific in all events (Santoso et al. 2017). For instance, SSTA is coupled with the surface zonal wind anomaly mainly through convective heating related to OLR anomalies. Similarly, thermocline (D20) fluctuation is driven by the zonal wind anomaly; then, through thermocline feedback, the D20 anomaly affects the SSTA. Such an interaction/coupling chain can start from anywhere on the loop. Moreover, zonal wind stress, subsurface ocean temperature (represented by D20), and atmospheric deep convection (represented by

OLR) anomalies also show some interesting differences not only between the strong and moderate–weak events but also among the four strong El Niños (Figs. 3a–d). For example, the positive anomaly of D20 in the eastern equatorial Pacific as well as the zonal gradient of the D20 anomaly between the eastern and western equatorial Pacific in their peak phases (Figs. 3a–d, contour) is the smallest during 2015/16 among the four events, the largest during 1997/98, and in between during 1982/83 and 1991/92. For the deep convection (OLR anomaly), it is stronger during 1982/83 and 1997/98, than during 1991/92 and 2015/16 (Figs. 3a–d, shading). Consistently, the surface zonal wind stress anomalies (Figs. 3a–d, vectors) are much stronger during 1997/98 than during the other three events. Furthermore, the location of the maximum convection anomaly is different. It is around  $150^{\circ}\text{W}$  during 1982/83 and 1997/98, and around  $165^{\circ}\text{W}$  during 1991/92 and 2015/16 (Figs. 3a–d, shading).

In addition, there are profound differences in the evolution of low-level winds (not anomalies) at 1000 hPa along the equator (averaged in  $5^{\circ}\text{S}$ – $5^{\circ}\text{N}$ ) in the four El

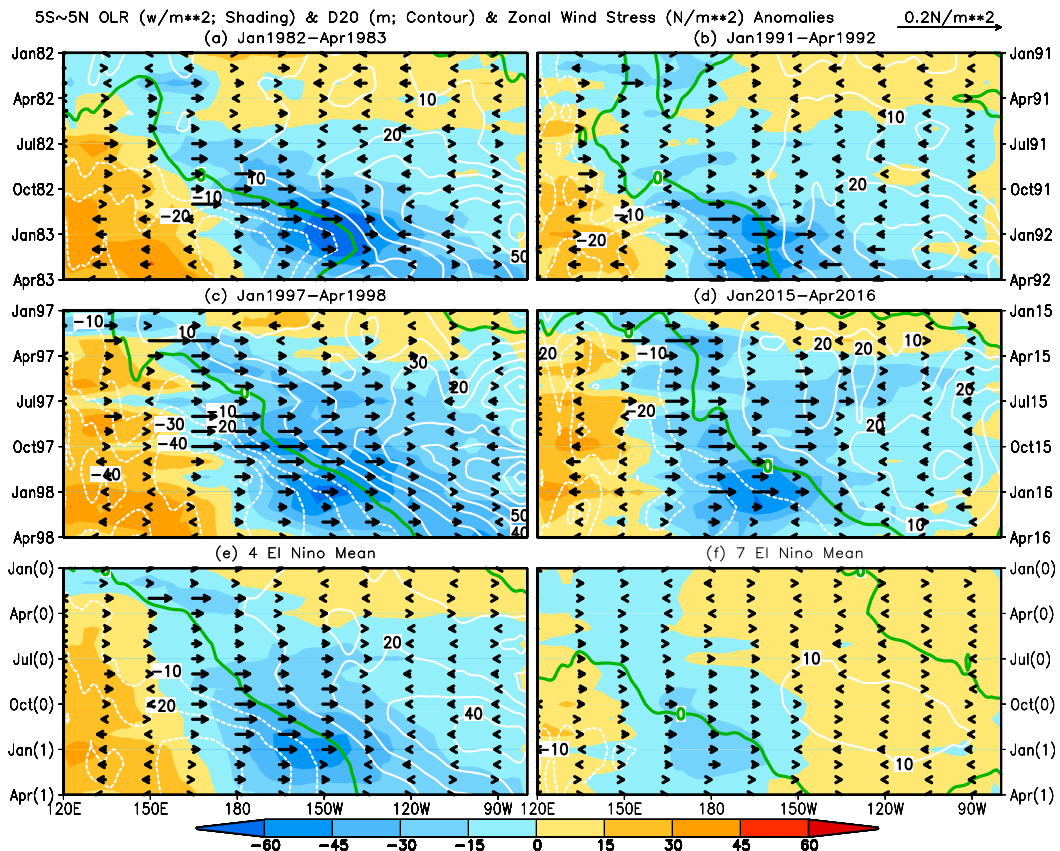


FIG. 3. Time evolution of monthly mean OLR (shading), D20 (contour), and zonal wind stress (vector) anomalies averaged in  $5^{\circ}\text{S}$ – $5^{\circ}\text{N}$  during (a) January 1982–April 1983, (b) January 1991–April 1992, (c) January 1997–April 1998, and (d) January 2015–April 2016 as well as the average for (e) the four strong El Niños and (f) seven weak–moderate El Niños. The unit is m for D20 and  $\text{W m}^{-2}$  for OLR. The contour interval is 10 m, and zero contour is dark green.

Niño events (Fig. 4). According to Hu and Fedorov (2016, their Fig. 1), total westerly wind is a good approximation of the westerly wind anomaly, and it is a good measurement for westerly wind bursts (WWBs). Here, WWB events can be identified as those episodes when westerly wind is larger than  $4 \text{ m s}^{-1}$  (Fig. 4, contour) and persists at least a few days (Tziperman and Yu 2007). The overall westerly wind is much stronger during 1997 than 1982, 1991, and 2015. In the development phase (e.g., spring–summer), WWBs are the strongest in 1997, the weakest in 1982, and in between in 1991 and 2015 (Fig. 4, contour). That means that WWBs appear earlier and stronger in the development phase of the 1997/98 event than that of 1982/83, 1991/92, and 2015/16 events. In autumn–winter, the westerly winds are strongest in 1997, weakest in 1991, and in between in 1982 and 2015. The differences of the low-level wind anomaly (e.g., WWB) may affect the atmosphere–ocean coupling associated with ENSO evolution (e.g., Penland and Sardeshmukh 1995; McPhaden 1999; Fedorov

2002; Lengaigne et al. 2002; Hu and Fedorov 2016; Puy et al. 2016; Chiodi and Harrison 2017), which is critical for ENSO diversity (Hu et al. 2012; Capotondi et al. 2015; Chen et al. 2015). For example, Hu et al. (2012) suggested that differences of zonal extension and intensity of westerly wind along the equatorial Pacific in the early months of a year is associated with different flavors of El Niño (Xie et al. 2015). Chen et al. (2015) argued that the asymmetry, irregularity, and extremes of El Niño result from WWBs and properly accounting for the interplay between the canonical cycle and WWBs may improve El Niño prediction.

Thus, although overall SSTA in the central and eastern equatorial Pacific is comparable between 1997/98 and 2015/16, the associated subsurface ocean temperature anomalies, as well as deep convection and surface wind stress anomalies in the central and eastern equatorial Pacific are much weaker during 2015/16 than during 1997/98. That may imply difference of atmosphere–ocean coupling as well as different contributions from different

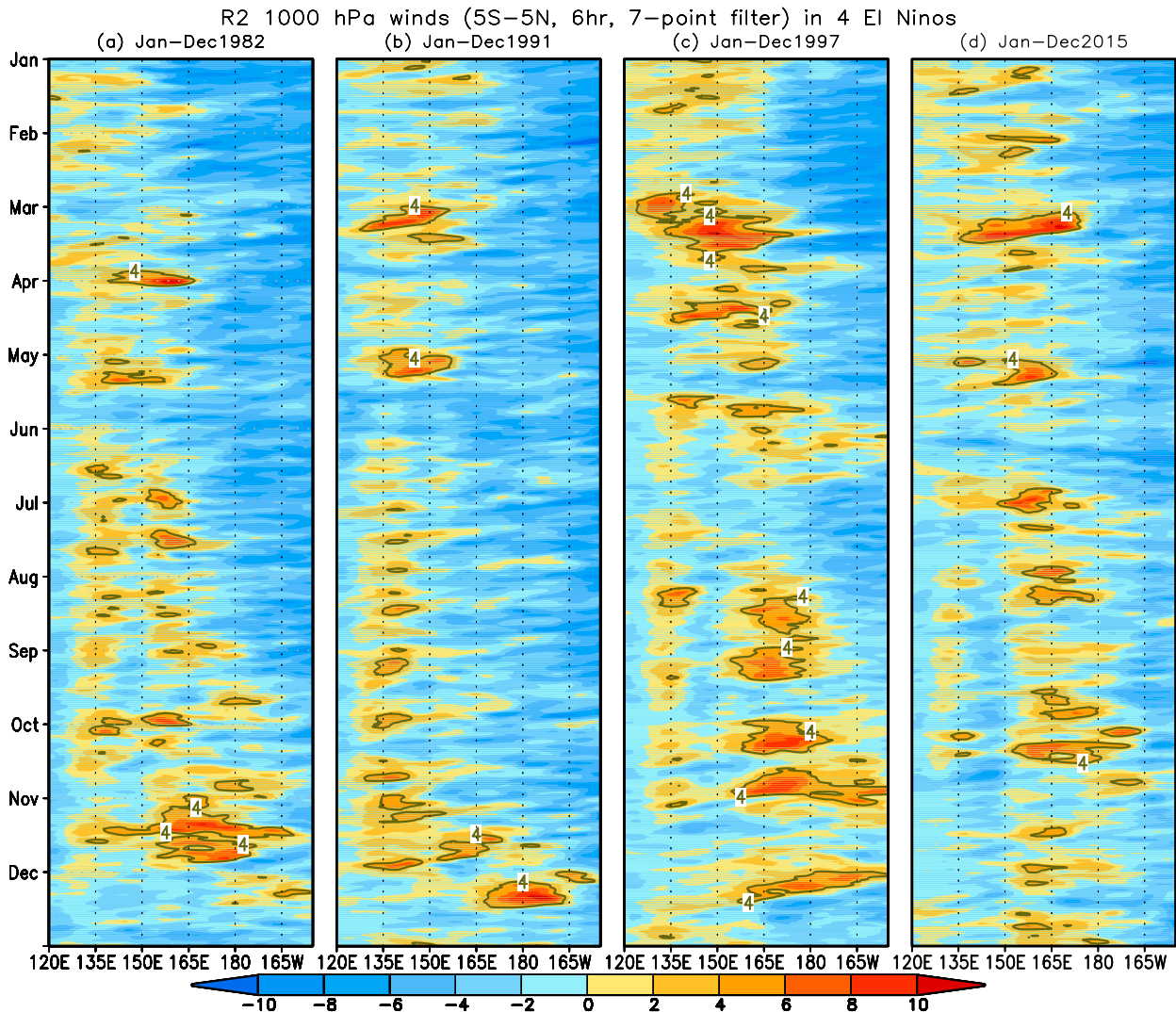


FIG. 4. Time evolution of westerly (red shading) and easterly (blue shading) wind (total) at 1000 hPa averaged in 5°S–5°N during (a) January–December 1982, (b) January–December 1991, (c) January–December 1997, and (d) January–December 2015. It is 6-hourly data and smoothed by 7-point running mean. The unit is  $\text{m s}^{-1}$ , and the contour represents  $4 \text{ m s}^{-1}$ .

time-scale components, which will be discussed in the following.

#### b. Contribution of atmosphere–ocean interaction

ENSO arises from atmosphere–ocean coupling (Bjerknes 1969). Such coupling involves surface wind and SST anomalies as well as thermocline fluctuation and plays a crucial role in the evolution of ENSO (Bjerknes 1969; Jin et al. 2006; Lloyd et al. 2009; Kim and Jin 2011). As an approximation, here, we use heat budget analysis of OML to represent the integrated atmosphere–ocean coupling associated with the growth and decay of ENSO. Figure 5 shows time-integrated ocean temperature anomalies caused by the individual terms in the heat budget of OML in the four events. We

note that both positive contribution from zonal and meridional advections, vertical entrainment and diffusion, and damping from thermodynamical processes are the strongest during 1997/98 (Fig. 5c), the weakest during 1982/83 (Fig. 5a), and in between during 1991/92 and 2015/16 (Figs. 5b,d). Compared with the 1982/83, 1991/92, and 1997/98 events, the maximum positive anomaly center of the dynamical terms and negative anomaly center of the thermodynamical terms are shifted farther westward in 2015/16. That is generally consistent with the corresponding longitude location contrast shown in other variables (Figs. 2, 3).

The weaker dynamical and thermodynamical term anomalies in 2015/16 imply weaker positive and negative feedbacks between the atmosphere and ocean

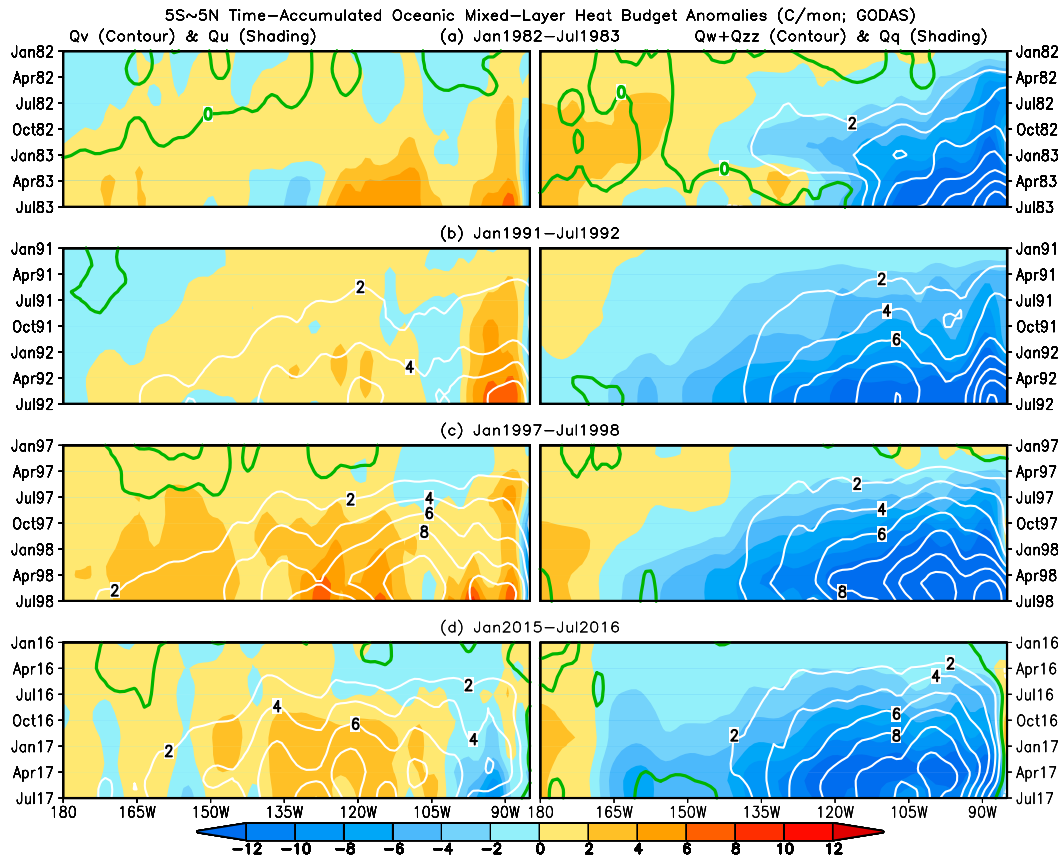


FIG. 5. (left) Time-accumulated zonal advection (shading) and meridional advection (contour) and (right) vertical entrainment and diffusion (contour) and surface heat flux (shading) terms of heat budget of OML averaged in 5°S–5°N during (a) January 1982–July 1983, (b) January 1991–July 1992, (c) January 1997–July 1998, and (d) January 2015–July 2016. The time accumulations of each term start from January 1982, January 1991, January 1997, and January 2015 in (a)–(d), respectively. The unit is °C month<sup>-1</sup>.

compared with 1997/98. The positive feedback between the ocean and atmosphere associated with ENSO is largely linked to the interaction between the surface wind and SST anomalies and between the surface wind anomaly and ocean thermocline slope fluctuation (e.g., Jin and An 1999). According to Lloyd et al. (2009), the wind–SST interaction can be approximately measured by the linear regression coefficient  $\alpha(x, y)$  of the zonal wind stress anomaly  $\tau_x(x, y, t)$  at every grid point  $(x, y)$  regressed against the Niño-3 SSTA, then averaged over the Niño region, which was also called Bjerknes feedback by Lloyd et al. (2009) or atmospheric Bjerknes feedback by Bellenger et al. (2014). The linear regression is expressed as

$$\tau_x(x, y, t) = \alpha(x, y) \times \text{Niño3}(t) + R(x, y, t).$$

Here,  $R(x, y, t)$  represents the residual.

Figure 6a shows the linear regression coefficients  $\alpha(x, y)$  of the zonal wind stress anomaly at every grid

point onto the Niño-3 SSTA during January 1981–December 2010, representing the climatological mean. It is seen that the pronounced positive feedback is mainly in the Niño-4 region (5°S–5°N, 160°E–150°W) and slightly shifted to the Southern Hemisphere, while negative feedback is mainly in 135°W eastward with reduced amplitude.

Here, we further compare the wind stress anomaly averaged in the Niño-3.4 region for linear regression projected part in the observation (Figs. 6b–e, shading) and the Niño-3.4 expected part based on the regression pattern from the Niño-3.4 index (Figs. 6b–e, solid line), as well as the observed average (Figs. 6b–e, dashed line) during the four El Niño events. The projected part is defined as  $\langle \tau_x(x, y, t) \times \alpha(x, y) \rangle / [\langle \alpha(x, y) \times \alpha(x, y) \rangle]^{0.5}$  and the Niño-3.4 expected part is referred to as  $\text{Niño-3.4} \times [\langle \alpha(x, y) \times \alpha(x, y) \rangle]^{0.5}$ , where  $\langle \rangle$  represents average in the Niño-3.4 region. The red (green) shading in Figs. 6b–e means that the zonal wind stress anomaly averaged in the Niño-3.4 region is larger

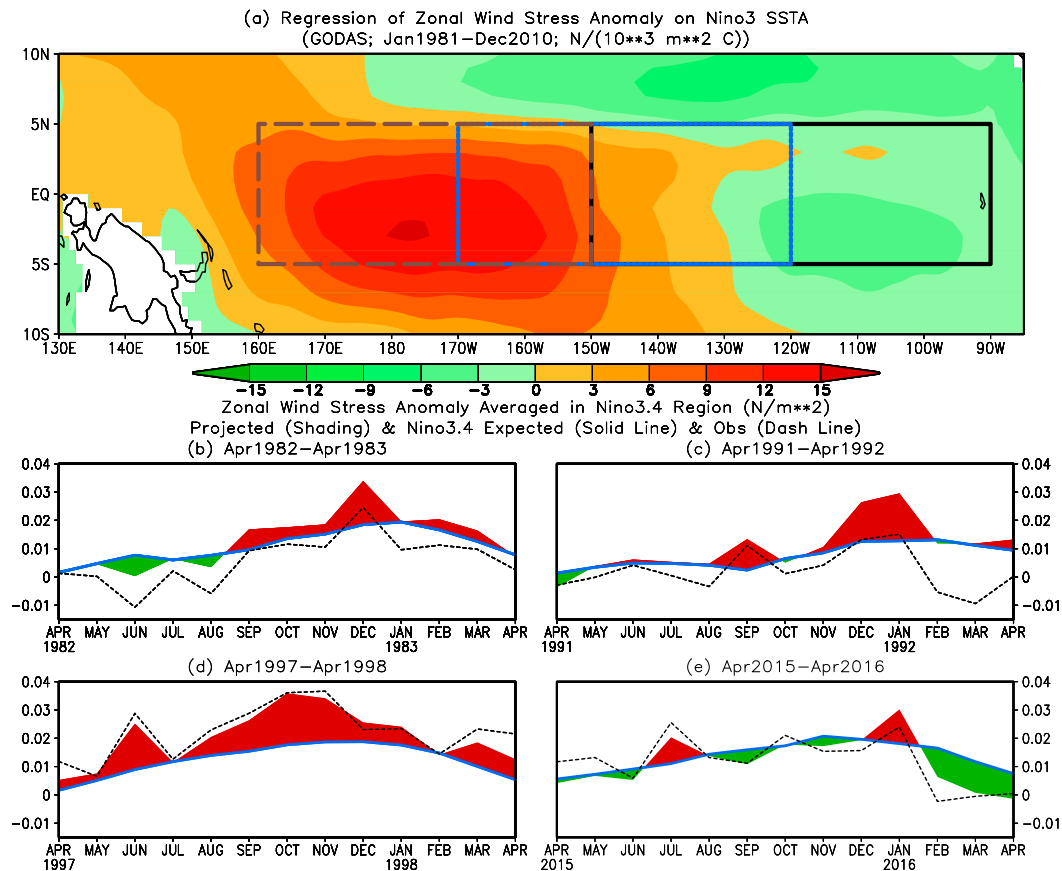


FIG. 6. (a) Linear regression of zonal wind stress anomaly onto Niño-3 SSTAs during January 1981–December 2010 and zonal wind stress anomaly averaged in the Niño-3.4 region for projected (shading), Niño-3.4 expected (solid line), and observed (dashed line) during (b) April 1982–April 1983, (c) April 1991–April 1992, (d) April 1997–April 1998, and (e) April 2015–April 2016. Red (green) shading means the projection is larger (smaller) than the Niño-3.4 expected zonal wind stress anomaly. The unit is  $N m^{-2}$  in (b)–(e). The rectangles in (a) represent the Niño-4, Niño-3.4, and Niño-3 regions, respectively.

(smaller) in the projection than in the Niño-3.4 expectation. That corresponds to excessive (deficient) zonal wind stress anomalies from linear regression, implying more (less) supportive zonal wind stress anomaly to the growth of ENSO SSTAs.

The zonal wind anomalies averaged in the Niño-3.4 region are comparable, and their evolutions are similar between the projection (shading) and observation (dashed lines) in each event (Figs. 6b–e), indicating that the linear regression projection largely reflects the observed zonal wind anomalies averaged in the Niño-3.4 region; also, they are varied simultaneously with the evolution of ENSO SSTAs (not shown). Examining the supportiveness of the zonal wind anomalies to the growth of ENSO SSTAs, we note that it is the most supportive during 1997/98 (Fig. 6d, most red shading), the least supportive during 2015/16 (Fig. 6e, least red shading and most green shading), and in between during

1982/83 and 1991/92 [Figs. 6b,c; e.g., more red (green) shading means more (less) supportive]. Thus, from the linear regression view, the observed wind anomaly is more supportive to the growth of ENSO SSTAs during 1997/98 than during 2015/16. Such supportive differences may come from either wind anomaly pattern and/or amplitude plus noise (WWB events) changes (Fig. 4).

Similarly, we calculate the linear regression of zonal wind stress anomalies onto the zonal gradient of the D20 anomaly, which is used to approximate the wind–thermocline interaction. The zonal gradient of the D20 anomaly is defined as the D20 anomaly between the eastern ( $5^{\circ}S$ – $5^{\circ}N$ ,  $150^{\circ}$ – $90^{\circ}W$ ; Fig. 7a, rectangle with dashed line) and western ( $5^{\circ}S$ – $5^{\circ}N$ ,  $120^{\circ}$ – $170^{\circ}E$ ; Fig. 7a, rectangle with solid line) equatorial Pacific. Such zonal gradient of the D20 anomaly is linked to the so-called tilt mode of thermocline variation or the slope variation of the thermocline along the equatorial Pacific and is in



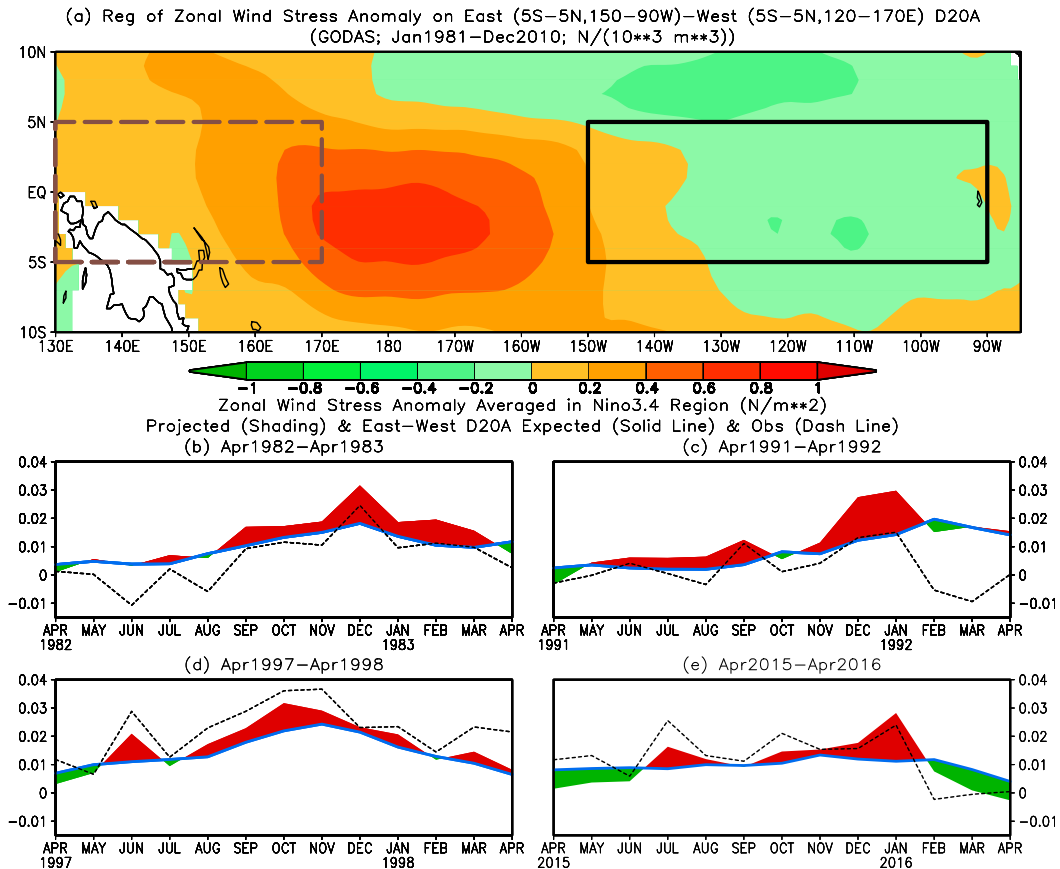


FIG. 7. As in Fig. 6, but for (a) linear regression of zonal wind stress anomaly onto the zonal gradient of the D20 anomaly between the eastern [5°S–5°N, 150°–90°W; rectangle with dashed line in (a)] and western [5°S–5°N, 120°–170°E; rectangle with solid line in (a)] equatorial Pacific during January 1981–December 2010 and zonal wind stress anomaly averaged in the Niño-3.4 region for projected (shading), zonal gradient of the D20 anomaly expected (solid line), and observed (dashed line) during (b) April 1982–April 1983, (c) April 1991–April 1992, (d) April 1997–April 1998, and (e) April 2015–April 2016. Red (green) shading means the projection is larger (smaller) than the expected zonal wind stress anomaly. The unit is  $N m^{-2}$  in (b)–(e).

balance with the zonal wind stress anomaly in the central equatorial Pacific, such as the Niño-3.4 region (Clarke 2010; Kumar and Hu 2014). According to Clarke (2010) and Kumar and Hu (2014, their Fig. 1a), the tilt mode varies in phase with ENSO (Niño-3.4 index). The regressions show a dipole pattern (Fig. 7a) with positive values in the western and central equatorial Pacific and negative ones (with smaller amplitudes) in the eastern, meaning that the positive (negative) zonal gradient of the D20 anomaly between the eastern and western equatorial Pacific is connected with the westerly (easterly) wind stress anomaly in the western and central equatorial Pacific and the easterly (westerly) anomaly in the eastern equatorial Pacific.

Similar to Figs. 6b–e, zonal wind anomalies averaged in the Niño-3.4 region are comparable and their evolutions are similar between projected (shading) and observed

(dashed lines) in each event (Figs. 7b–e), implying that the linear regression projection largely reflects the observed zonal wind anomalies averaged in the Niño-3.4 region. Overall, the zonal gradient of the D20 anomaly expected zonal wind stress anomalies (solid lines) are smaller than the projected (shading) for all the events, suggesting excessive zonal wind stress anomalies in driving the thermocline dipole-like oscillation between the eastern and western equatorial Pacific. Interestingly, the observed wind stress anomaly is clearly larger than the projected and expected ones during 1997/98, a unique feature among the four events. Compared with the zonal wind stress anomaly associated with the zonal gradient of D20 anomalies (both projected and expected), it is noted that it is the smallest in the 2015/16 El Niños among the four events (Figs. 7b–e). This suggests that the zonal wind stress anomaly in the

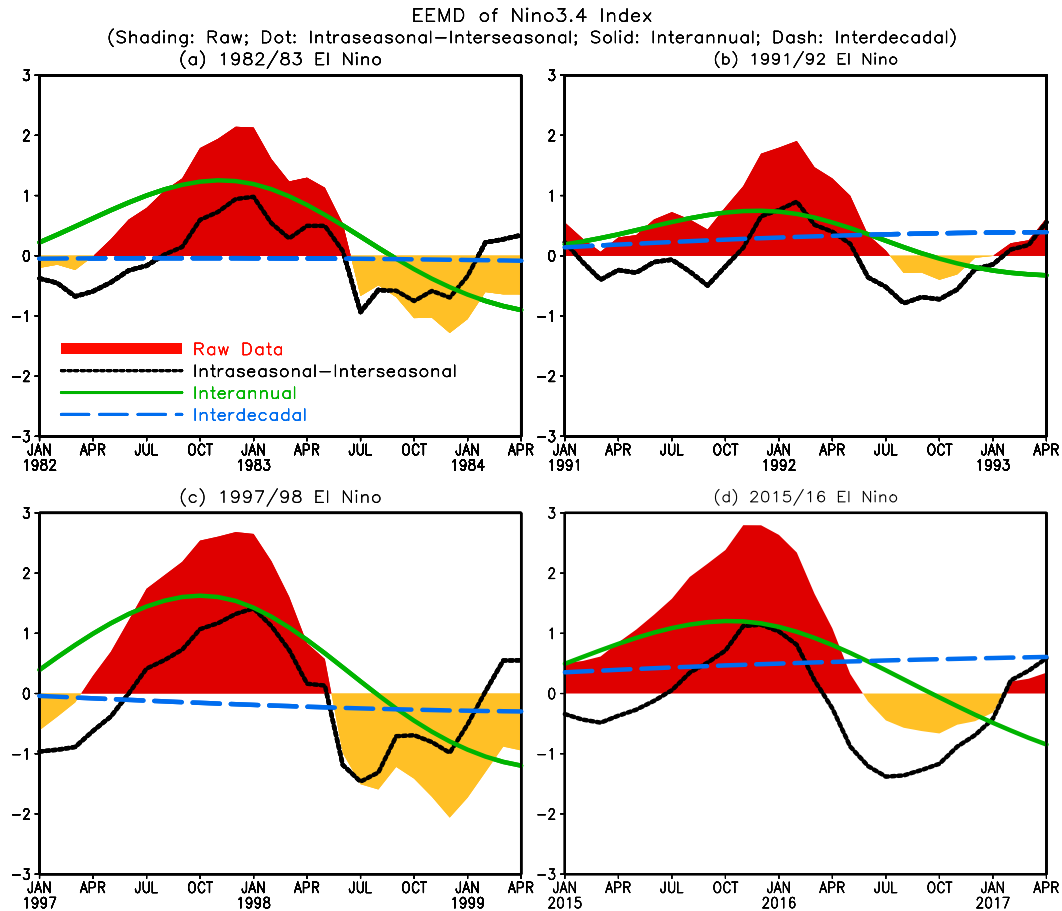


FIG. 8. Monthly mean Niño-3.4 SSTA during (a) January 1982–April 1984, (b) January 1991–April 1993, (c) January 1997–April 1999, and (d) January 2015–April 2017. Shading is raw data, and dotted/black, solid/green, and dashed/blue lines represent EEMD components at intraseasonal–interseasonal, interannual, and interdecadal and longer time scales, respectively.

central equatorial Pacific is less supportive to the thermocline dipole-like oscillation in 2015/16 El Niño compared with that in the other three events, consisting with the D20 anomaly evolution shown in Fig. 3.

Through examining the contributions of the atmosphere–ocean coupling (wind–SST and wind–thermocline interactions) to El Niño–associated SSTA in the four strong El Niños, we note that the relative importance of the atmosphere–ocean coupling to El Niño–associated SSTA growth varies with event. Compared with the 1997/98 El Niño, the weaker wind–SST and wind–thermocline interactions in the 2015/16 El Niño seem unable to explain their comparable intensity. That may imply that in addition to the wind–SST and wind–thermocline interactions, other factors contribute to the strength of El Niño–associated SSTAs, particularly for the 2015/16 El Niño. One of the potential factors may be associated with differences of the contribution of different time-scale

variations in different El Niño events. That will be discussed in the next subsection.

### c. Contribution of low-frequency variations

In addition to intraseasonal–interannual variations associated with atmosphere–ocean coupling, interdecadal variation and long-term-trend background may also contribute to the observed SSTA evolution and ENSO intensity shown in Fig. 1 (Barnett 1991; Yeo et al. 2017). To examine contributions of different time-scale variation to the observed Niño-3.4 SSTA, EEMD is conducted. Figure 8 displays raw Niño-3.4 SSTA (shading), its components at intraseasonal–interseasonal (dotted line; time scales shorter than 1 year), interannual (solid line; time scales between 1 and 10 years), and interdecadal-trend (dashed line; time scales longer than 10 years) time scales in the four strong El Niño events. The interannual component (solid line) is always positive, since ENSO in nature is an interannual time-scale phenomena. Also,

the intraseasonal–interseasonal time-scale component (dotted line) always has a positive contribution to growth of all the four strong El Niños.

Interestingly, the interdecadal-trend time-scale components (Fig. 8, dashed line) have different contributions to the amplitudes of Niño-3.4 SSTAs (or the intensity) of the various El Niños. Contribution from the interdecadal-trend time-scale variation is ignorable during the 1982/83 El Niño and negative during the 1997/98 El Niño. But the contributions are notably positive during the 1991/92 and 2015/16 El Niños. The contribution is especially large during the 2015/16 El Niño, and the three time-scale (intraseasonal–interseasonal, interannual, and interdecadal trend) variations have nearly comparable contributions to the observed Niño-3.4 SSTA in its peak phase. This is consistent with the fact that the 2015/16 warm event spanned a longer period than the 1982/83 and 1997/98 events if we count the warm SSTAs in the tropical Pacific during most of 2014. Although the warm anomalies in 2014 were relatively weak, they did make the equatorial Pacific relatively warm so that the Niño-3.4 index was close to  $0.5^{\circ}\text{C}$  in January 2015 (Fig. 1, blue curve), while the Niño-3.4 indices in the corresponding month for the 1982/83 (black curve) and 1997/98 (green curve) events were negative. Therefore, the higher “initial” value played a role in making the 2015/16 event a strong El Niño, even though its growth rate in the summer and fall of 2015 was smaller than those of the 1982/83 and 1997/98 events (Levine and McPhaden 2016).

Nevertheless, it should be pointed out that the contribution of the interdecadal and longer time-scale component to the amplitude of ENSO depends on the referred base period. For example, with the base period of 1872–2015 and by applying cyclostationary empirical orthogonal function analysis (Kim 2002), Yeo et al. (2017) noted that a secular warming trend had positive contributions to all three strong El Niños (1982/83, 1997/98, and 2015/16), and the contribution is much larger to the 2015/16 than to the 1982/83 El Niños (Yeo et al. 2017, their Figs. 3, 5). In this work, the referred base period is 1981–2010; thus, a large portion of the trend shown in Yeo et al. (2017) was eliminated.

Therefore, in addition to the atmosphere–ocean coupling at intraseasonal to interannual time scales, interdecadal and longer time-scale variation largely enhances the amplitude of 2015/16 El Niño. As a result, the amplitudes of El Niño are comparable in 1997/98 and 2015/16 (Huang et al. 2016), although the atmosphere–ocean coupling is weaker in 2015/16 than in 1997/98 (Figs. 6, 7). The contrary contributions of the interdecadal and longer time-scale variations to Niño-3.4 SSTAs on the

other hand imply their importance in determining the amplitude/intensity of an ENSO event (Hu et al. 2012; L’Heureux et al. 2013; Jha et al. 2014). The North Pacific and Atlantic Oceans have been suggested as two sources of the multidecadal variability described here (Verdon and Franks 2006; Yu et al. 2015; Levine et al. 2017; Lin et al. 2018).

#### 4. Summary and discussion

In this work, we examine the evolution of oceanic and atmospheric anomalies in the equatorial Pacific during four strong El Niños (1982/83, 1991/92, 1997/98, and 2015/16) since 1979. Then contributions of the atmosphere–ocean coupling to El Niño–associated SSTA during the four strong El Niños are identified. Furthermore, low-level winds, as well as time-scale dependence of Niño-3.4 SSTAs are examined to understand their differences of relative importance of the atmosphere–ocean coupling in different El Niño events.

Among the four strong El Niños, overall SSTAs in the central and eastern equatorial Pacific are stronger during the 1997/98 and 2015/16 El Niños than during 1982/83 and 1991/92. Nevertheless, the associated subsurface ocean temperature anomalies, as well as deep convection and surface wind stress anomalies in the central and eastern equatorial Pacific are weaker during 2015/16 than during 1997/98. That implies differences of atmosphere–ocean coupling strength that is confirmed by the differences of the wind–SST and wind–thermocline interactions in different events. The relative importance of the wind–SST and wind–thermocline interactions to El Niño–associated SSTA growth depends on the El Niño event. Both the wind–SST and wind–thermocline interactions play a less important role during 2015/16 than during the 1997/98 El Niños. Such differences may be associated with differences of the low-level westerly wind as well as the contribution of different time-scale variations in an event.

Similar to the interannual time-scale variation, the intraseasonal–interseasonal time-scale component always has positive contribution to the growth of all the four strong El Niños. Interestingly, the interdecadal-trend time-scale component plays a different role in different events. The contribution is ignorable during the 1982/83 El Niño, negative during the 1997/98 El Niño, and notably positive during the 1991/92 and 2015/16 El Niños. The contribution of the interdecadal time-scale component is especially large during the 2015/16 El Niño, and the three time-scale (intraseasonal–interseasonal, interannual, and interdecadal trend) variations have nearly comparable contribution to the observed Niño-3.4 SSTA in

its peak phase. The interdecadal-trend time-scale variations may be associated with the interdecadal shift of ENSO around 1999/2000 (Hu et al. 2016, 2017); nevertheless, it is unclear what caused the shift. Therefore, although the atmosphere–ocean coupling seems weaker in 2015/16 than in 1997/98, the comparable amplitude of the two events is because the interdecadal-trend components enhanced the amplitude in 2015/16 and depressed the amplitude in 1997/98. Thus, in addition to the atmosphere–ocean coupling at intraseasonal to interannual time scales, low-frequency (interdecadal and longer time scale) variation is important and sometimes crucial in determining or modulating the intensity of an ENSO event.

Last, here the analyses focus on comparison of strong El Niños by using one oceanic reanalysis (GODAS) and one atmospheric reanalysis (NCEP–DOE). In fact, the uncertainties or biases in different reanalyses are sometime tremendous (Xue et al. 2011), even for the air–sea coupling processes associated with ENSO (Kumar and Hu 2012), the strongest interseasonal–interannual variability in the global ocean. Such uncertainties and biases are expected to affect the quantitative results of the comparison. That is a future research topic.

*Acknowledgments.* Authors appreciate the constructive comments and suggestions from Professor Fei-Fei Jin and two other anonymous reviewers. The procedure of the heat budget calculation used in this work was developed by Dr. Boyin Huang and is maintained by Dr. C. Wen. For data used in this study, please contact us via xiaofanli@zju.edu.cn. This work was supported by National Natural Science Foundation of China (41775040 and 41475039) and National Key Basic Research and Development Project of China (2015CB953601). Bohua Huang is supported by grants from NSF (AGS-1338427), NASA (NNX14AM19G), and NOAA (NA14OAR4310160 and NA17OAR4310144). The scientific results and conclusions, as well as any view or opinions expressed herein, are those of the authors and do not necessarily reflect the views of NWS, NOAA, or the Department of Commerce.

#### REFERENCES

- An, S.-I., and J.-W. Kim, 2017: Role of nonlinear ocean dynamic response to wind on the asymmetrical transition of El Niño and La Niña. *Geophys. Res. Lett.*, **44**, 393–400, <https://doi.org/10.1002/2016GL071971>.
- Ashok, K., S. K. Behera, S. A. Rao, H. Weng, and T. Yamagata, 2007: El Niño Modoki and its possible teleconnection. *J. Geophys. Res.*, **112**, C11007, <https://doi.org/10.1029/2006JC003798>.
- Barnett, T. P., 1991: The interaction of multiple time scales in the tropical climate system. *J. Climate*, **4**, 269–285, [https://doi.org/10.1175/1520-0442\(1991\)004<0269:TOMTS>2.0.CO;2](https://doi.org/10.1175/1520-0442(1991)004<0269:TOMTS>2.0.CO;2).
- Barnston, A. G., M. K. Tippett, M. L. L’Heureux, S. Li, and D. G. DeWitt, 2012: Skill of real-time seasonal ENSO model predictions during 2002–11: Is our capability increasing? *Bull. Amer. Meteor. Soc.*, **93**, 631–651, <https://doi.org/10.1175/BAMS-D-11-00111.1>.
- Behringer, D. W., 2007: The Global Ocean Data Assimilation System (GODAS) at NCEP. *11th Symp. on Integrated Observing and Assimilation Systems for Atmosphere, Oceans, and Land Surface*, San Antonio, TX, Amer. Meteor. Soc., 3.3, [http://ams.confex.com/ams/87ANNUAL/techprogram/paper\\_119541.htm](http://ams.confex.com/ams/87ANNUAL/techprogram/paper_119541.htm).
- Bellenger, H., E. Guilyardi, J. Leloup, M. Lengaigne, and J. Vialard, 2014: ENSO representation in climate models: From CMIP3 to CMIP5. *Climate Dyn.*, **42**, 1999–2018, <https://doi.org/10.1007/s00382-013-1783-z>.
- Bjerknes, J., 1969: Atmospheric teleconnections from the equatorial Pacific. *Mon. Wea. Rev.*, **97**, 163–172, [https://doi.org/10.1175/1520-0493\(1969\)097<0163:ATFTEP>2.3.CO;2](https://doi.org/10.1175/1520-0493(1969)097<0163:ATFTEP>2.3.CO;2).
- Capotondi, A., and Coauthors, 2015: Understanding ENSO diversity. *Bull. Amer. Meteor. Soc.*, **96**, 921–938, <https://doi.org/10.1175/BAMS-D-13-00117.1>.
- Chen, D., and Coauthors, 2015: Strong influence of westerly wind bursts on El Niño diversity. *Nat. Geosci.*, **8**, 339–345, <https://doi.org/10.1038/ngeo2399>.
- Chiodi, A. M., and D. E. Harrison, 2017: Observed El Niño SSTa development and the effects of easterly and westerly wind events in 2014/15. *J. Climate*, **30**, 1505–1519, <https://doi.org/10.1175/JCLI-D-16-0385.1>.
- Clarke, A. J., 2010: Analytical theory for the quasi-steady and low-frequency equatorial ocean response to wind forcing: The “tilt” and “warm water volume” modes. *J. Phys. Oceanogr.*, **40**, 121–137, <https://doi.org/10.1175/2009JPO4263.1>.
- Fedorov, A. V., 2002: The response of the coupled tropical ocean–atmosphere to westerly wind bursts. *Quart. J. Roy. Meteor. Soc.*, **128**, 1–23, <https://doi.org/10.1002/qj.200212857901>.
- Hu, S., and A. V. Fedorov, 2016: Exceptional strong easterly wind burst stalling El Niño of 2014. *Proc. Natl. Acad. Sci. USA*, **113**, 2005–2010, <https://doi.org/10.1073/pnas.1514182113>.
- Hu, Z.-Z., A. Kumar, B. Jha, W. Wang, B. Huang, and B. Huang, 2012: An analysis of warm pool and cold tongue El Niños: Air–sea coupling processes, global influences, and recent trends. *Climate Dyn.*, **38**, 2017–2035, <https://doi.org/10.1007/s00382-011-1224-9>.
- , —, and B. Huang, 2016: Spatial distribution and the interdecadal change of leading modes of heat budget of the mixed-layer in the tropical Pacific and the association with ENSO. *Climate Dyn.*, **46**, 1753–1768, <https://doi.org/10.1007/s00382-015-2672-4>.
- , —, —, J. Zhu, and H.-L. Ren, 2017: Interdecadal variations of ENSO around 1999/2000. *J. Meteor. Res.*, **31**, 73–81, <https://doi.org/10.1007/s13351-017-6074-x>.
- , —, J. Zhu, P. Peng, and B. Huang, 2019: On the challenge for ENSO cycle prediction: An example from NCEP Climate Forecast System, version 2. *J. Climate*, **32**, 183–194, <https://doi.org/10.1175/JCLI-D-18-0285.1>.
- Huang, B., C.-S. Shin, J. Shukla, L. Marx, M. A. Balmaseda, S. Halder, P. A. Dirmeyer, and J. L. Kinter III, 2017: Reforecasting the ENSO events in the past 57 years (1958–2014). *J. Climate*, **30**, 7669–7693, <https://doi.org/10.1175/JCLI-D-16-0642.1>.
- Huang, B., Y. Xue, D. Zhang, A. Kumar, and M. J. McPhaden, 2010: The NCEP GODAS ocean analysis of the tropical Pacific mixed layer heat budget on seasonal to interannual time scales. *J. Climate*, **23**, 4901–4925, <https://doi.org/10.1175/2010JCLI3373.1>.

- , M. L'Heureux, J. Lawrimore, C. Liu, H.-M. Zhang, V. Banzon, Z.-Z. Hu, and A. Kumar, 2013: Why did large differences arise in the sea surface temperature datasets across the tropical Pacific during 2012? *J. Atmos. Oceanic Technol.*, **30**, 2944–2953, <https://doi.org/10.1175/JTECH-D-13-00034.1>.
- , —, Z.-Z. Hu, and H.-M. Zhang, 2016: Ranking the strongest ENSOs while incorporating SST uncertainty. *Geophys. Res. Lett.*, **43**, 9165–9172, <https://doi.org/10.1002/2016GL070888>.
- Huang, N. E., and Z. Wu, 2008: A review on Hilbert-Huang transform: The method and its applications on geophysical studies. *Rev. Geophys.*, **46**, RG2006, <https://doi.org/10.1029/2007RG000228>.
- , and Coauthors, 1998: The empirical mode decomposition and the Hilbert spectrum for nonlinear and non-stationary time series analysis. *Proc. Roy. Soc. London*, **454A**, 903–993, <https://doi.org/10.1098/rspa.1998.0193>.
- Jha, B., Z.-Z. Hu, and A. Kumar, 2014: SST and ENSO variability and change simulated in historical experiments of CMIP5 models. *Climate Dyn.*, **42**, 2113–2124, <https://doi.org/10.1007/s00382-013-1803-z>.
- Jin, F.-F., 1997a: An equatorial ocean recharge paradigm for ENSO. Part I: Conceptual model. *J. Atmos. Sci.*, **54**, 811–829, [https://doi.org/10.1175/1520-0469\(1997\)054<0811:AEORPF>2.0.CO;2](https://doi.org/10.1175/1520-0469(1997)054<0811:AEORPF>2.0.CO;2).
- , 1997b: An equatorial ocean recharge paradigm for ENSO. Part II: A stripped-down coupled model. *J. Atmos. Sci.*, **54**, 830–847, [https://doi.org/10.1175/1520-0469\(1997\)054<0830:AEORPF>2.0.CO;2](https://doi.org/10.1175/1520-0469(1997)054<0830:AEORPF>2.0.CO;2).
- , and S.-I. An, 1999: Thermocline and zonal advective feedbacks within the equatorial ocean recharge oscillator model for ENSO. *Geophys. Res. Lett.*, **26**, 2989–2992, <https://doi.org/10.1029/1999GL002297>.
- , S. T. Kim, and L. Bejarano, 2006: A coupled-stability index of ENSO. *Geophys. Res. Lett.*, **33**, L23708, <https://doi.org/10.1029/2006GL027221>.
- Kanamitsu, M., W. Ebisuzaki, J. Woolen, S.-K. Yang, J. J. Hnilo, M. Fiorino, and G. L. Potter, 2002: NCEP–DOE AMIP-II Reanalysis (R-2). *Bull. Amer. Meteor. Soc.*, **83**, 1631–1643, <https://doi.org/10.1175/BAMS-83-11-1631>.
- Kao, H.-Y., and J.-Y. Yu, 2009: Contrasting eastern-Pacific and central-Pacific types of ENSO. *J. Climate*, **22**, 615–632, <https://doi.org/10.1175/2008JCLI2309.1>.
- Kim, K.-Y., 2002: Investigation of ENSO variability using cyclostationary EOFs of observational data. *Meteor. Atmos. Phys.*, **81**, 149–168, <https://doi.org/10.1007/s00703-002-0549-7>.
- Kim, S. T., and F.-F. Jin, 2011: An ENSO stability analysis. Part I: Results from a hybrid coupled model. *Climate Dyn.*, **36**, 1593–1607, <https://doi.org/10.1007/s00382-010-0796-0>.
- Kug, J.-S., J. Choi, S.-I. An, F.-F. Jin, and A. T. Wittenberg, 2010: Warm pool and cold tongue El Niño events as simulated by the GFDL 2.1 coupled GCM. *J. Climate*, **23**, 1226–1239, <https://doi.org/10.1175/2009JCLI3293.1>.
- Kumar, A., and Z.-Z. Hu, 2012: Uncertainty in the ocean–atmosphere feedbacks associated with ENSO in the reanalysis products. *Climate Dyn.*, **39**, 575–588, <https://doi.org/10.1007/s00382-011-1104-3>.
- , and —, 2014: Interannual variability of ocean temperature along the equatorial Pacific in conjunction with ENSO. *Climate Dyn.*, **42**, 1243–1258, <https://doi.org/10.1007/s00382-013-1721-0>.
- , and M. Chen, 2017: What is the variability in US West Coast winter precipitation during strong El Niño events? *Climate Dyn.*, **49**, 2789–2802, <https://doi.org/10.1007/s00382-016-3485-9>.
- , —, Y. Xue, and D. Behringer, 2015: An analysis of the temporal evolution of ENSO prediction skill in the context of the equatorial Pacific Ocean observing system. *Mon. Wea. Rev.*, **143**, 3204–3213, <https://doi.org/10.1175/MWR-D-15-0035.1>.
- Lengaigne, M., J.-P. Boulanger, C. Menkes, S. Masson, G. Madec, and P. Delecluse, 2002: Ocean response to the March 1997 westerly wind event. *J. Geophys. Res.*, **107**, 8015, <https://doi.org/10.1029/2001JC000841>.
- Levine, A. F. Z., and M. J. McPhaden, 2016: How the July 2014 easterly wind burst gave the 2015–2016 El Niño a head start. *Geophys. Res. Lett.*, **43**, 6503–6510, <https://doi.org/10.1002/2016GL069204>.
- , —, and D. M. W. Frierson, 2017: The impact of the AMO on multidecadal ENSO variability. *Geophys. Res. Lett.*, **44**, 3877–3886, <https://doi.org/10.1002/2017GL072524>.
- L'Heureux, M., D. C. Collins, and Z.-Z. Hu, 2013: Linear trends in sea surface temperature of the tropical Pacific Ocean and implications for the El Niño–Southern Oscillation. *Climate Dyn.*, **40**, 1223–1236, <https://doi.org/10.1007/s00382-012-1331-2>.
- Liang, P., Z.-Z. Hu, Y. Liu, X. Yuan, X. Li, and X. Jiang, 2019: Challenges in predicting and simulating summer rainfall in the eastern China. *Climate Dyn.*, <https://doi.org/10.1007/s00382-018-4256-6>, in press.
- Liebmann, B., and C. A. Smith, 1996: Description of a complete (interpolated) outgoing longwave radiation dataset. *Bull. Amer. Meteor. Soc.*, **77**, 1275–1277.
- Lim, Y.-K., R. M. Kovach, S. Pawson, and G. Vernieres, 2017: The 2015/16 El Niño event in context of the MERRA-2 reanalysis: A comparison of the tropical Pacific with 1982/83 and 1997/98. *J. Climate*, **30**, 4819–4842, <https://doi.org/10.1175/JCLI-D-16-0800.1>.
- Lin, R., F. Zheng, and X. Dong, 2018: ENSO frequency asymmetry and the Pacific decadal oscillation in observations and 19 CMIP5 models. *Adv. Atmos. Sci.*, **35**, 495–506, <https://doi.org/10.1007/s00376-017-7133-z>.
- Lloyd, J., E. Guilyardi, H. Weller, and J. Slingo, 2009: The role of atmosphere feedbacks during ENSO in the CMIP3 models. *Atmos. Sci. Lett.*, **10**, 170–176, <https://doi.org/10.1002/asl.227>.
- McPhaden, M. J., 1999: Genesis and evolution of the 1997–98 El Niño. *Science*, **283**, 950–954, <https://doi.org/10.1126/science.283.5404.950>.
- National Research Council, 2010: *Assessment of Intraseasonal to Interannual Climate Prediction and Predictability*. National Academies Press, 192 pp.
- Paek, H., J.-Y. Yu, and C. Qian, 2017: Why were the 2015/16 and 1997/98 extreme El Niños different? *Geophys. Res. Lett.*, **44**, 1848–1856, <https://doi.org/10.1002/2016GL071515>.
- Penland, C., and P. D. Sardeshmukh, 1995: The optimal growth of tropical sea surface temperature anomalies. *J. Climate*, **8**, 1999–2024, [https://doi.org/10.1175/1520-0442\(1995\)008<1999:TOGOTS>2.0.CO;2](https://doi.org/10.1175/1520-0442(1995)008<1999:TOGOTS>2.0.CO;2).
- Philander, S. G. H., 1990: *El Niño, La Niña and the Southern Oscillation*. Academic Press, 293 pp.
- Puy, M., J. Vialard, M. Lengaigne, and E. Guilyardi, 2016: Modulation of equatorial Pacific westerly/easterly wind events by the Madden–Julian Oscillation and convectively-coupled Rossby waves. *Climate Dyn.*, **46**, 2155–2178, <https://doi.org/10.1007/s00382-015-2695-x>.
- Rasmusson, E. M., and T. H. Carpenter, 1982: Variation in tropical sea surface temperature and surface wind fields associated with Southern Oscillation/El Niño. *Mon. Wea.*

- Rev., **110**, 354–384, [https://doi.org/10.1175/1520-0493\(1982\)110<0354:VITSST>2.0.CO;2](https://doi.org/10.1175/1520-0493(1982)110<0354:VITSST>2.0.CO;2).
- Ren, H.-L., R. Wang, P. Zhai, Y. Ding, and B. Lu, 2017: Upper-ocean dynamical features and prediction of the super El Niño in 2015/16: A comparison with the cases in 1982/83 and 1997/98. *J. Meteor. Res.*, **31**, 278–294, <https://doi.org/10.1007/s13351-017-6194-3>.
- Reynolds, R. W., N. A. Rayner, T. M. Smith, D. C. Stokes, and W. Wang, 2002: An improved in situ and satellite SST analysis for climate. *J. Climate*, **15**, 1609–1625, [https://doi.org/10.1175/1520-0442\(2002\)015<1609:AIISAS>2.0.CO;2](https://doi.org/10.1175/1520-0442(2002)015<1609:AIISAS>2.0.CO;2).
- Ropelewski, C. F., and M. S. Halpert, 1987: Global and regional scale precipitation patterns associated with the El Niño/Southern Oscillation. *Mon. Wea. Rev.*, **115**, 1606–1626, [https://doi.org/10.1175/1520-0493\(1987\)115<1606:GARSPP>2.0.CO;2](https://doi.org/10.1175/1520-0493(1987)115<1606:GARSPP>2.0.CO;2).
- Santoso, A., M. J. McPhaden, and W. Cai, 2017: The defining characteristics of ENSO extremes and the strong 2015/2016 El Niño. *Rev. Geophys.*, **55**, 1079–1129, <https://doi.org/10.1002/2017RG000560>.
- Sarachik, E. S., and M. A. Cane, 2010: *The El Niño–Southern Oscillation Phenomenon*. Cambridge University Press, 384 pp.
- Tseng, Y.-H., R. Ding, and X.-M. Huang, 2017: The warm blob in the northeast Pacific—The bridge leading to the 2015/16 El Niño. *Environ. Res. Lett.*, **12**, 054019, <https://doi.org/10.1088/1748-9326/aa67c3>.
- Tziperman, E., and L. Yu, 2007: Quantifying the dependence of westerly wind bursts on the large-scale tropical Pacific SST. *J. Climate*, **20**, 2760–2768, <https://doi.org/10.1175/JCLI4138a.1>.
- Verdon, D. C., and S. W. Franks, 2006: Long-term behavior of ENSO: Interactions with the PDO over the past 400 years inferred from paleoclimate records. *Geophys. Res. Lett.*, **33**, L06712, <https://doi.org/10.1029/2005GL025052>.
- Wang, C., 2001: A unified oscillator model for the El Niño–Southern Oscillation. *J. Climate*, **14**, 98–115, [https://doi.org/10.1175/1520-0442\(2001\)014<0098:AUOMFT>2.0.CO;2](https://doi.org/10.1175/1520-0442(2001)014<0098:AUOMFT>2.0.CO;2).
- Wang, H., A. Kumar, and W. Wang, 2013: Characteristics of subsurface ocean response to ENSO assessed from simulations with the NCEP Climate Forecast System. *J. Climate*, **26**, 8065–8083, <https://doi.org/10.1175/JCLI-D-12-00795.1>.
- Wang, W., M. Chen, and A. Kumar, 2010: An assessment of the CFS real-time seasonal forecasts. *Wea. Forecasting*, **25**, 950–969, <https://doi.org/10.1175/2010WAF2222345.1>.
- Wu, R., Z.-Z. Hu, and B. P. Kirtman, 2003: Evolution of ENSO-related rainfall anomalies in East Asia. *J. Climate*, **16**, 3742–3758, [https://doi.org/10.1175/1520-0442\(2003\)016<3742:EOERAI>2.0.CO;2](https://doi.org/10.1175/1520-0442(2003)016<3742:EOERAI>2.0.CO;2).
- Wu, Z., and N. E. Huang, 2009: Ensemble empirical mode decomposition: A noise-assisted data analysis method. *Adv. Adapt. Data Anal.*, **1**, 1–41, <https://doi.org/10.1142/S1793536909000047>.
- Xie, R., F. Huang, F.-F. Jin, and J. Huang, 2015: The impact of basic state on quasi-biennial periodicity of central Pacific ENSO over the past decade. *Theor. Appl. Climatol.*, **120**, 55–67, <https://doi.org/10.1007/s00704-014-1150-y>.
- Xue, Y., B. Huang, Z.-Z. Hu, A. Kumar, C. Wen, D. Behringer, and S. Nadiga, 2011: An assessment of oceanic variability in the NCEP Climate Forecast System Reanalysis. *Climate Dyn.*, **37**, 2511–2539, <https://doi.org/10.1007/s00382-010-0954-4>.
- Yeo, S.-R., S.-W. Yeh, K.-Y. Kim, and W. Kim, 2017: The role of low frequency variation in the manifestation of warming trend and ENSO amplitude. *Climate Dyn.*, **49**, 1197–1213, <https://doi.org/10.1007/s00382-016-3376-0>.
- Yu, J.-Y., P.-K. Kao, H. Paek, H.-H. Hsu, C.-W. Hung, M.-M. Lu, and S.-I. An, 2015: Linking emergence of the central Pacific El Niño to the Atlantic multidecadal oscillation. *J. Climate*, **28**, 651–662, <https://doi.org/10.1175/JCLI-D-14-00347.1>.
- Zhang, R.-H., F. Zheng, J. Zhu, and Z. Wang, 2013: A successful real-time forecast of the 2010–11 La Niña event. *Sci. Rep.*, **3**, 1108, <https://doi.org/10.1038/srep01108>.
- Zheng, Z., Z.-Z. Hu, and M. L’Heureux, 2016: Predictable components of ENSO evolution in real-time multi-model predictions. *Sci. Rep.*, **6**, 35909, <https://doi.org/10.1038/srep35909>.
- Zhu, J., A. Kumar, B. Huang, M. A. Balmaseda, Z.-Z. Hu, L. Marx, and J. L. Kinter III, 2016: The role of off-equatorial surface temperature anomalies in the 2014 El Niño prediction. *Sci. Rep.*, **6**, 19677, <https://doi.org/10.1038/srep19677>.